Analyst

PAPER

View Article Online
View Journal | View Issue

Cite this: *Analyst*, 2015, **140**, 3143

Microbial respiration and natural attenuation of benzene contaminated soils investigated by cavity enhanced Raman multi-gas spectroscopy

Tobias Jochum,[a] Beate Michalzik,[b] Anne Bachmann,[a] Jürgen Popp[a,c,d] and Torsten Frosch*[a,c]

Soil and groundwater contamination with benzene can cause serious environmental damage. However, many soil microorganisms are capable to adapt and are known to strongly control the fate of organic contamination. Innovative cavity enhanced Raman multi-gas spectroscopy (CERS) was applied to investigate the short-term response of the soil micro-flora to sudden surface contamination with benzene regarding the temporal variations of gas products and their exchange rates with the adjacent atmosphere. ^{13}C-labeled benzene was spiked on a silty-loamy soil column in order to track and separate the changes in heterotrophic soil respiration – involving $^{12}CO_2$ and O_2 – from the natural attenuation process of benzene degradation to ultimately form $^{13}CO_2$. The respiratory quotient (RQ) decreased from a value 0.98 to 0.46 directly after the spiking and increased again within 33 hours to a value of 0.72. This coincided with the maximum $^{13}CO_2$ concentration rate (0.63 μmol m^{-2} s^{-1}), indicating the highest benzene degradation at 33 hours after the spiking event. The diffusion of benzene in the headspace and the biodegradation into $^{13}CO_2$ were simultaneously monitored and 12 days after the benzene spiking no measurable degradation was detected anymore. The RQ finally returned to a value of 0.96 demonstrating the reestablished aerobic respiration.

Received 15th January 2015,
Accepted 25th February 2015

DOI: 10.1039/c5an00091b

www.rsc.org/analyst

Introduction

Monitored natural attenuation refers "to the reliance on natural attenuation processes (within the context of a carefully controlled and monitored site cleanup approach) to achieve site-specific remediation objectives within a time frame that is reasonable compared to that offered by other more active methods", according to U.S. EPA.[1] Other terms associated with natural attenuation include for instance "intrinsic remediation or bioremediation", "passive bioremediation", "natural recovery", and "natural assimilation". These natural processes are used to reduce the concentration and amount of pollutants in contaminated soils and groundwater, encompassing microbial biodegradation, dispersion, dilution, volatilization and contaminant sorption onto soil solids. As a low cost means compared to thermal and other physico-chemical techniques, natural attenuation has become of widespread interest.[2–4] However, to test the effectiveness of natural attenuation processes and the underlying mechanisms under varying physico-chemical conditions and indigenous microflora, the contamination needs to be carefully monitored through the process.[5,6] Benzene, as an important component of gasoline and a widespread precursor in the chemical industry, is a major organic pollutant in soils and groundwater. Due to its toxicity as a carcinogenic and teratogenic agent, detailed characterization of possible benzene decontamination by microbial remediation processes is required in order to estimate the soil quality and the effectiveness of decontamination. One approach for elucidating the metabolic pathways of this degradation is the quantification of the gas exchange rates between the soil and the atmosphere.

The most commonly used sensing technique for environmental gas analysis is lab-based gas chromatography,[7] usually coupled with mass spectrometry[8] or flame ionization detection.[9] Although highly sensitive and selective, this technique is slow, sample consumptive and limited in terms of mobility. Infrared (IR) absorption spectroscopy methods[10–12] feature very high sensitivities for molecules with a permanent dipole moment, such as carbon dioxide or methane, down to the ppm and ppb range.[13] However, IR based techniques are not

[a]*Leibniz Institute of Photonic Technology, Jena, Germany.*
E-mail: torsten.frosch@uni-jena.de, torsten.frosch@gmx.de; Tel: +49 3641 206221
[b]*Friedrich Schiller University, Institute of Geography, Jena, Germany*
[c]*Friedrich Schiller University, Institute for Physical Chemistry, Jena, Germany*
[d]*Friedrich Schiller University, Abbe Center of Photonics, Jena, Germany*

suitable for the detection of crucial homonuclear atmospheric gases like N_2 or O_2. Particularly, quantifying dioxygen consumption rates is fundamental for calculating the respiratory quotient (RQ) and thus deducing the microbial activity.[14] Raman spectroscopy is an emerging technique,[15–18] based on molecular vibrations,[19–21] and offers the ability for simultaneous and selective multi-gas quantification. Almost all gases and volatiles, except for the noble gases, can be detected and quantified with only a single measurement.[22–24] As a fast, sensitive and non-consumptive technique, Raman spectroscopy promises great potential for onsite environmental gas analysis and process monitoring.[25,26]

Materials and methods

Soil characterization

The sampling of top soil material (0–10 cm depth) was conducted in May 2014 from a grassland plot close to Kammerforst, Hainich-Dün region in the western part of the federal state of Thuringia, central Germany. The climate exhibited an annual precipitation of 750–800 mm and an annual average air temperature of 6.8 °C (44.2 °F). The bedrock consists of Triassic shell limestone covered by a Pleistocene loess layer of variable thickness forming soils classified as Stagnosols and Luvisols.[27] For the determination of the organic carbon (C_{org}) and total nitrogen (TN) content and the soil pH, the air dried samples were sieved through a <2 mm sieve. Soil pH was measured in the supernatant of a 1 : 2.5 mixture of soil and deionized water using a glass electrode (WTW Multi 340i with SenTix41–3 electrode, Weilheim). Oven-dried subsamples for the elemental analysis were homogenized, ground and passed through a 40 μm sieve. The total carbon and nitrogen concentrations were determined by thermal oxidation (Trumac Elementaranalyzer, Leco). After removal of inorganic carbon by repeated washing with 10% hydrogen chloride (HCl), organic carbon was quantified with the same elemental analyzer. The soil texture was determined by laser diffraction particle size analysis (Laser Diffraction Particle Size Analyzer, Beckman Coulter). Table 1 summarizes the soil parameters.

Gas analysis

An innovative Raman gas sensor[28,29] was applied and adapted for the gas measurements reported here. It is based on a miniaturized laser diode ($\lambda_{excitation}$ = 650 nm, 50 mW), which is frequency locked and feedback-coupled to a power buildup cavity[30] to achieve a power enhancement of 5 orders of magnitude. This enhancement enables monitoring of gas concentrations down to approximately 50 ppm within one second. For a direct quantification of the different multi-gas compounds the pressure, temperature and laser intensity were monitored by additional sensors. The setup was calibrated with the relevant gases, namely nitrogen N_2, oxygen O_2, ^{13}C-labeled benzene $^{13}C_6H_6$, and the carbon dioxide isotopes $^{12}CO_2$ and $^{13}CO_2$. Here, pure $^{13}C_6H_6$ was cooled to 7 °C during the calibration to reduce its vapor pressure. By using the Clausius–Clapeyron relationship within the ideal gas approximation at low temperatures,

$$\ln\frac{p_2}{p_1} = \frac{L}{R}\left(\frac{1}{T_1} - \frac{1}{T_2}\right), \quad (1)$$

the gaseous benzene concentration could be directly linked to the Raman signal intensity and hence be calibrated. Here, the two sets p_1, T_1 and p_2, T_2 define the thermodynamic states 1 and 2 by their pressure and temperature, respectively. R is the universal gas constant and L the enthalpy of vaporization, which was assumed to be constant. A least squares fit of the experimental multi-gas spectrum was performed with the complete set of individually calibrated pure reference spectra in the wavenumber range from 500 to 3000 cm^{-1}. This fitting procedure reveals the concentrations of the particular gas components and is more precise than integrating only the specific peak areas. In addition, temperature induced wavenumber shifts were precisely corrected by a custom-made software routine.

Any difference between the measured spectrum and the convoluted calibration spectra also unveils the presence of unexpected, and not calibrated gases. These additional unexpected gases can also be quantified by adding their calibration spectra in the least square fit, which illustrates the versatility of the setup to address not only predetermined gases. All the above-mentioned gases can be distinguished without cross-sensitivity by their individual spectral shifts in the acquired Raman spectrum; an exemplary multi-gas spectrum is depicted in Fig. 1A. The two carbon dioxide isotopes, $^{12}CO_2$ and $^{13}CO_2$, can be distinguished and simultaneously be quantified due to their deviance in the Fermi dyad (Fig. 1B). The calibration data sets were proved in test measurements with defined gas compositions mixed by mass flow controllers. The obtained gas concentrations were normalized for a constant sum of all gas concentrations.

Experimental design

The field-fresh soil was acclimatized to 21 °C in a climate chamber one day before beginning the experiment. 200 g of the soil were filled in a custom-built Plexiglas column (V = 295 cm^3) and sealed airtight with a screw-in lid enclosing a septum (Fig. 2). In order to establish a reproducible gas composition, the soil headspace (V = 98 cm^3) was flushed with synthetic air (20% O_2, 80% N_2, Linde, Germany), precisely controlled by using a mass flow controller (MFC, Brooks Instrument, Germany). During flushing, the gases were quanti-

Table 1 Soil parameters. The top soil was sampled from a grassland plot in the Hainich-Dün region, Thuringia, Germany

Soil texture						
Clay (%)	Silt (%)	Sand (%)	pH (H_2O)	C_{org} (%)	TN (%)	C/N
18.1	81.3	0.6	4.87	2.35	0.221	10.65

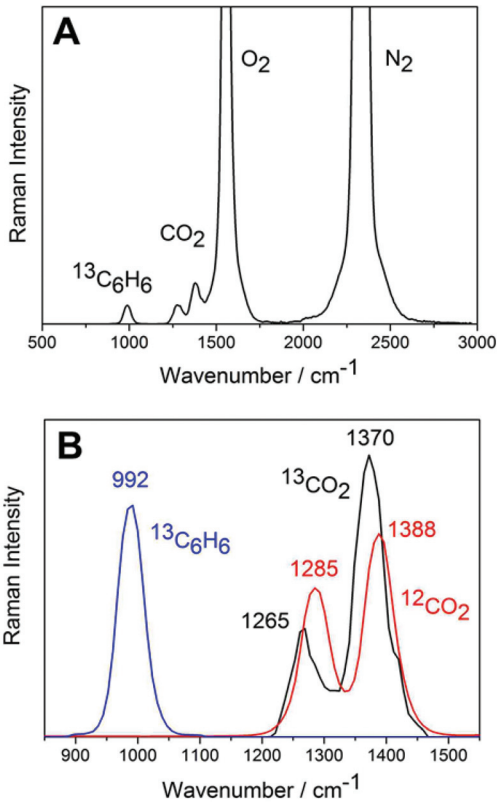

Fig. 1 (A) Example of an experimental multi-gas Raman spectrum ($\lambda_{excitation}$ = 650 nm) during the natural attenuation experiment. Most prominent are the rotation-vibrational bands of N_2 (2331 cm^{-1}) and O_2 (1556 cm^{-1}), both with unresolved O and S branches. The concentrations of the individual components were calculated by least-square fitting the multi-gas spectrum with the particular calibration spectra. (B) Due to their deviance in the Fermi dyad, the two carbon dioxide isotopes $^{12}CO_2$ (red) and $^{13}CO_2$ (black) can be distinguished. Also depicted is the $^{13}C_6H_6$ mode at 992 cm^{-1} (blue).

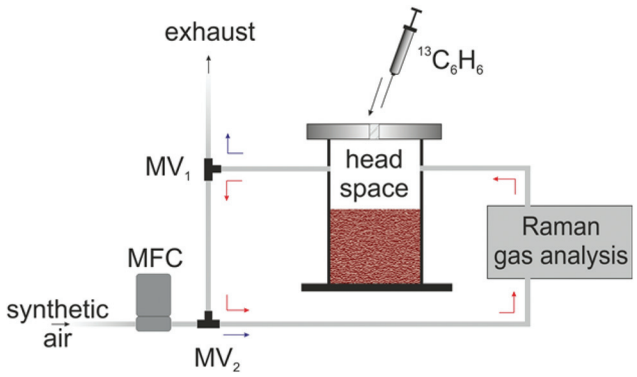

Fig. 2 Schematic diagram of the experimental setup, consisting of mass flow controller (MV), magnetic valves (MV_1 and MV_2), soil mesocosm, and Raman gas analyzer. The gas flow paths during rate measurement and flushing are indicated by red and blue arrows, respectively. All gas rates were determined within the closable inner cycle, comprising the soil column and the Raman gas sensor. Using a syringe, the soil was spiked once with ^{13}C-labeled benzene and the gas exchange was monitored afterwards.

fied and left as exhaust. After a selected time of 150 seconds, the magnetic valves (MV) were switched and the inner circuit with the soil column and the Raman gas sensor was closed. A custom-made LabView routine was used for automatic operation of the MVs, the MFCs, and the Raman gas spectrometer. The current headspace gas composition was permanently monitored by the Raman gas sensor. Due to the aerobic soil respiration (here the carbohydrate model)

$$C_6H_{12}O_6 + 6O_2 \rightarrow 6CO_2 + 6H_2O, \quad (2)$$

the $^{12}CO_2$ concentration in the headspace increased with time.

To avoid any inhibition of this natural process, for instance by back-diffusion into the soil, the $^{12}CO_2$ concentration had to be kept within an environmentally adequate concentration window. Therefore, by reaching a preset $^{12}CO_2$ concentration threshold of 600 ppm, the magnetic valves were switched automatically back to their former state for 150 seconds (feedback control), such that the headspace was flushed with synthetic air again. This eventually reduced the $^{12}CO_2$ concentration in the headspace to approximately 100 ppm and the gas dynamics could be monitored once more afterwards. Using the slope of a linear regression of an individual gas concentration with respect to the time, the respective gas exchange rates could be determined (Fig. 3). Here, each fit was only applied for the first 30 minutes of a period between two flushing events in order to stay within the linear flux regime.[31] The rates were normalized by the column surface area of 19.6 cm^2. The microbial respiratory behavior and the natural attenuation characteristics were confirmed in a follow-up experiment under the same conditions (data not shown).

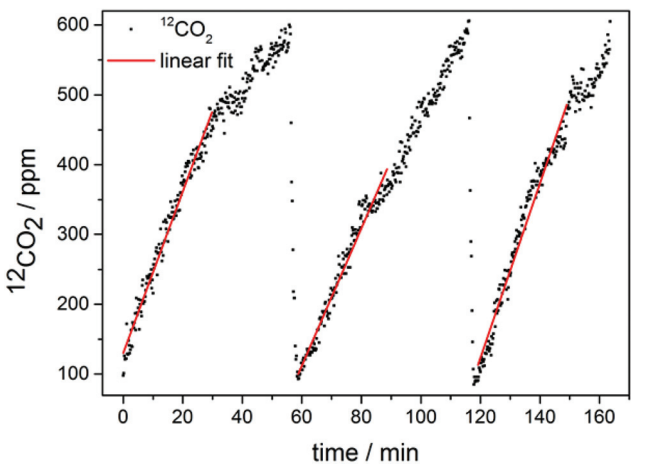

Fig. 3 Exemplary quantification of the $^{12}CO_2$ production rates. The change in concentration (black) with respect to time is linearly fitted (red). The linear regression is limited to the first 30 minutes of each cycle to stay within the linear regime. The slopes of the linear fits yielded the respective $^{12}CO_2$ gas exchange rates. Other gas rates were calculated accordingly. For better visualization, the time scale in this plot starts at zero-time, which does not match the experimental time scale in this case.

Results and discussion

Gas exchange rates

As mentioned above, the gas exchange rates of the bare, undisturbed soil were analyzed at first (indicated as negative time values in Fig. 4). The mean $^{12}CO_2$ concentration rate was 0.72 (±0.01) μmol m^{-2} s^{-1}, while the mean O_2 concentration rate amounted to −0.74 (±0.02) μmol m^{-2} s^{-1}. The respiratory quotient (RQ), defined as the molar ratio of the produced units of CO_2 per consumed unit of O_2, yielded 0.98 (±0.03) on average. This mirrors the case of aerobic soil respiration,[32] where the CO_2 evolution and the O_2 uptake are equimolar (eqn (2)). After measuring several gas exchange rates of the bare soil, the center of the soil surface was spiked with 0.1 ml pure labeled benzene $^{13}C_6H_6$ (Sigma-Aldrich, Germany) using a syringe penetrating the septum (Fig. 2). The syringe was immediately removed after the injection and the septum additionally sealed. Directly after surface spiking, exponential benzene diffusion in the gas phase was observed, different from other models assuming a subsurface contaminant injection.[33] Thus, the first post-spiking rates of CO_2 and O_2 in the gas phase were determined 30 minutes after spiking, such that abrupt non-equilibrium diffusion processes did not interfere with these acquired rates. Benzene was oxidized by the soil microorganisms to carbon dioxide and water *via*[34]

$$^{13}C_6H_6 + 7.5O_2 \rightarrow 6\ ^{13}CO_2 + 3H_2O. \quad (3)$$

Hence, for each mol of degraded benzene $^{13}C_6H_6$, 6 mol of $^{13}CO_2$ were produced. This enabled the calculation of the total amount of degraded benzene by measuring the headspace $^{13}CO_2$ concentration. Directly after the injection of benzene at time zero, a huge microbial response became apparent (Fig. 4). The $^{12}CO_2$ and O_2 concentration rates were remarkably increased up to 1.79 and −3.89 μmol m^{-2} s^{-1}, respectively. This strong response in microbial respiration is assumed to result from a phenomenon known as the "Birch effect"[35,36] describing a rapid release of carbon dioxide from the re-wetted soil material. The spiking resulted in an RQ of 0.46, which corresponds to the reported RQ values of about 0.4 after the addition of hexadecane to agricultural and forest soils.[37] On the one hand, this might be due to the metabolization of those deceased microorganisms,[38] which have been most directly exposed to the spiked benzene (caused by heterotrophic microflora); on the other hand, from microbial stress demanding more energy for cell repair mechanisms.[39] Within the first hours, the two rates dropped rapidly and the oxygen rate reached a minimum of −0.46 μmol m^{-2} s^{-1} 15 hours after

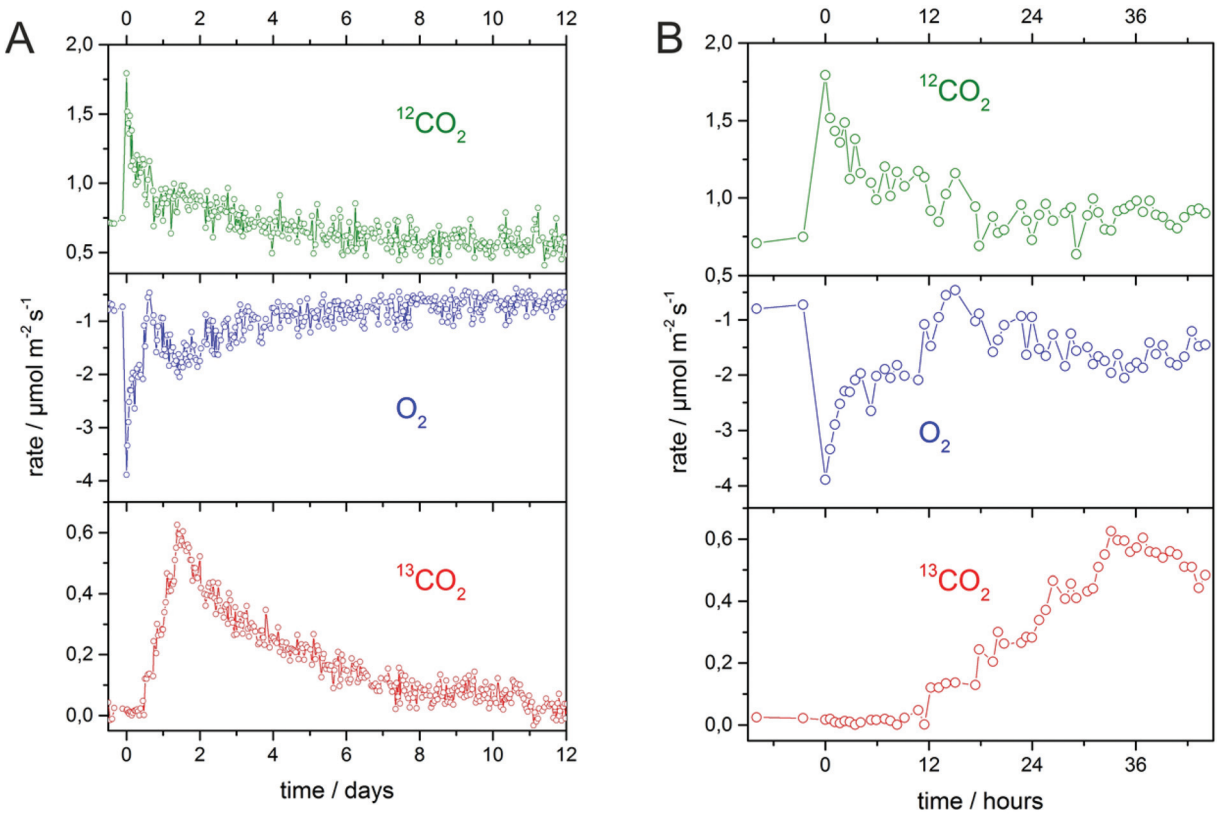

Fig. 4 (A) Evolution of the $^{12}CO_2$ (top), O_2 (center) and $^{13}CO_2$ (bottom) rates. Negative times correspond to the pre-spiking phase. (B) Detailed view onto the first 45 hours of the experiment after spiking.

spiking. During this decrease, both gas rates stabilized approximately from 3.5 to 11.5 hours after spiking; the $^{12}CO_2$ rate at 1.1 μmol m^{-2} s^{-1} and the O_2 rate at −2.0 μmol m^{-2} s^{-1}. However, the $^{13}CO_2$ rate remained unaffected within the first 12 hours, indicating that no measurable degradation of the labeled benzene took place. While the $^{12}CO_2$ rate decreased further after 15 hours, the O_2 rate increased again. This contrast behavior coincided with the emergence of the $^{13}CO_2$ production, demonstrating the initiated degradation of the labeled benzene, which accompanies an increased oxygen demand.

The maximum $^{13}CO_2$ rate of 0.63 μmol m^{-2} s^{-1} was reached 33 hours after spiking. This time corresponds with the reported time windows after application of D-glucose on soils[40] or benzene to pure cultures isolated from soils.[41] On the other hand, the observed 33 hours until maximum degradation was reached, differ from the reported – typically longer – times in cases when benzene[42] or hydrocarbons[43] were thoroughly mixed with the complete soil mass. After 34 hours – about the same time as the $^{13}CO_2$ production rate reached the maximum, – the O_2 consumption rate peaked at −2.06 μmol m^{-2} s^{-1} depicting again the correlation of $^{13}CO_2$ production and O_2 uptake. An RQ of 0.72 was measured at the time of highest $^{13}CO_2$ rates 33 hours after spiking, which is in good agreement with the theoretical RQ of 0.8 during benzene degradation, obtained by the stoichiometric eqn (3). The concentrations of all three gas rates – $^{12}CO_2$, O_2 and $^{13}CO_2$ – decreased continuously during the rest of the experiment. The $^{13}CO_2$ production disappeared 12 days after the spiking event. At the end of the experiment, the mean $^{12}CO_2$ rate amounted to 0.58 (±0.02) μmol m^{-2} s^{-1} and the mean O_2 rate was −0.63 (±0.03) μmol m^{-2} s^{-1}. These rates were slightly lower than the respective pre-spiking rates. This suggests that the microbes perished partly due to the lethal impact of benzene, which then resulted in a lowered overall microbial respiratory activity. A mean RQ of 0.96 (±0.04) was reached 12 days after the spiking event. Thus, the soil returned to the characteristic aerobic respiration following eqn (2).

Benzene fate

The benzene diffusion into the atmosphere was further investigated in order to quantify the degradation process. Utilizing the online multi-gas detection ability provided by the CERS sensor, the headspace concentration of the labeled benzene $^{13}C_6H_6$ was continuously monitored and analyzed. Due to its high vapor pressure (approximately 10.4 kPa at 21 °C)[44] and the direct surface application by the spiking, most of the benzene evaporated and diffused into the headspace. Diffused benzene was calculated by measuring the difference of initial and final concentrations during the flushing events, because of the observed non-linearity of the benzene flux. $^{13}C_6H_6$ diffusion dropped exponentially, which is in good agreement with theoretical calculations.[45] The total amount of diffused benzene is depicted in Fig. 5A. After 4 hours already half of the added benzene passed into the gaseous phase. The strong diffusion ended after almost 6.5 days. By then, 1025 μmol $^{13}C_6H_6$ diffused in total, which corresponds to 91.4% of the spiked mass. The total amount of degraded benzene was calculated by integration of the $^{13}CO_2$ production rates. Because 6 carbon dioxide molecules were produced per consumed benzene molecule, the total amount of degraded $^{13}C_6H_6$ could be directly evaluated (Fig. 5B). After a lag time of 12 hours, $^{13}CO_2$ was monitored in the column headspace, indicating the advent of the degradation process. Approximately 40 μmol $^{13}C_6H_6$ were degraded after 12 days, which was equivalent to 3.6% of the spiked benzene. Thus in total, 95% of the added $^{13}C_6H_6$ found its way into the headspace after 12 days, either by diffusion or degraded into $^{13}CO_2$. Several studies on transport and diffusion of organic compounds in unsaturated soil columns[46,47] suggest that the remainder most likely diffused into subjacent soil layers. These mechanisms will be studied in more detail (*e.g.* under varying benzene concentrations and soil pH) in further experiments.

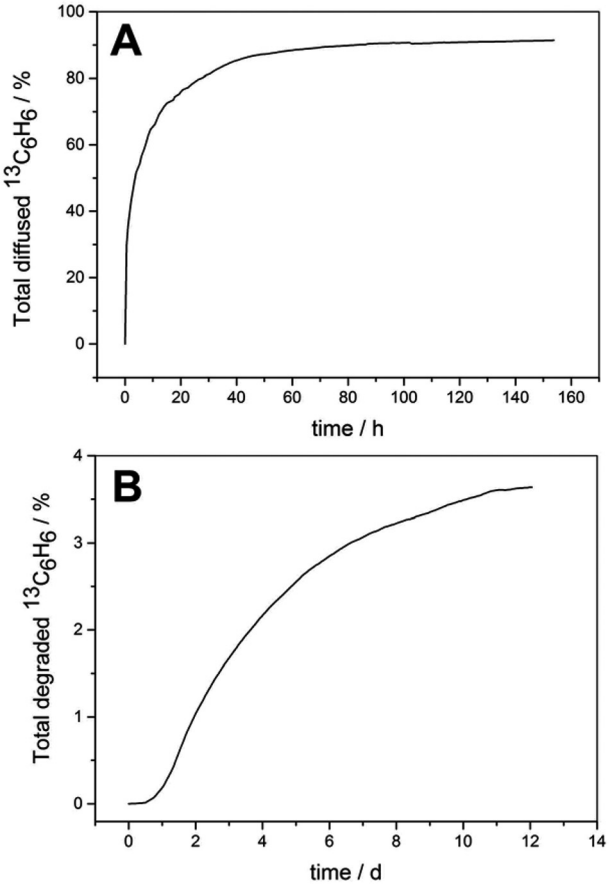

Fig. 5 (A) Diffusion of the spiked benzene from the soil surface into the headspace. (B) Biodegradation dynamics of benzene. The total amount of degraded benzene was calculated by integration of the $^{13}CO_2$ production rates.

Conclusion

In summary, cavity enhanced Raman gas sensing was demonstrated as a supremely versatile technique for online monitor-

ing of multi-gas compositions consisting of $^{12}CO_2$, $^{13}CO_2$, O_2, and $^{13}C_6H_6$ with just one single measurement. The application of CERS is non-consumptive, such that continuous and quantitative gas measurements are feasible, while preventing manipulations of the gas composition. The high temporal resolution and automated design of the Raman gas setup enabled the analysis of rapid gas dynamics and the elucidation of the accompanying chemical processes behind them. In this work, CERS was applied for the quantification of the natural attenuation of ^{13}C-labeled benzene after superficial application on a silty-loamy soil surface, representing sudden contamination events *e.g.* at petrol stations or industrial plants. The impact of benzene spiking on the microbial respiratory activity was investigated. The monitored RQ effectively indicated the subsequent microbial phases: first the aerobic pre-spiking respiration (RQ value of almost 1), the immediate response to the benzene application (with low RQ values and an increased oxygen demand), than the maximum degradation phase (with a RQ of 0.72 close to the theoretical value) and eventually the return to the aerobic respiration again. Considering the unique versatility and selectivity of cavity enhanced Raman gas sensing and its high potential for miniaturization, we foresee that CERS will develop into an important technique for the gas analysis of contaminated soils.

Acknowledgements

The authors kindly acknowledge the support by the Collaborative Research Centre AquaDiva, funded by the German Science Foundation (SFB 1076). We thank Robert Keiner for advice on Raman sensor operation.

Notes and references

1 U. S. EPA, Use of monitored natural attenuation at superfund, RCRA corrective action and underground storage tank sites, OSWER Directive Number 9200.4-17P, Office of Solid Waste and Emergency Response, Washington, DC, 1999.
2 H. Rugner, M. Finkel, A. Kaschl and M. Bittens, *Environ. Sci. Policy*, 2006, **9**, 568–576.
3 M. Tyagi, M. M. R. da Fonseca and C. C. C. R. de Carvalho, *Biodegradation*, 2011, **22**, 231–241.
4 M. Megharaj, B. Ramakrishnan, K. Venkateswarlu, N. Sethunathan and R. Naidu, *Environ. Int.*, 2011, **37**, 1362–1375.
5 C. N. Mulligan and R. N. Yong, *Environ. Int.*, 2004, **30**, 587–601.
6 E. Jindrova, M. Chocova, K. Demnerova and V. Brenner, *Folia Microbiol.*, 2002, **47**, 83–93.
7 B. Michalzik and B. Stadler, *Basic Appl. Ecol.*, 2000, **1**, 117–123.
8 J. F. Pankow, W. Luo, A. N. Melnychenko, K. C. Barsanti, L. M. Isabelle, C. Chen, A. B. Guenther and T. N. Rosenstiel, *Atmos. Meas. Tech.*, 2012, **5**, 345–361.
9 M. Deppe, K. H. Knorr, D. M. McKnight and C. Blodau, *Biogeochemistry*, 2010, **100**, 89–103.
10 O. Heinemeyer, H. Insam, E. A. Kaiser and G. Walenzik, *Plant Soil*, 1989, **116**, 191–195.
11 J. Iqbal, M. J. Castellano and T. B. Parkin, *Global Change Biol.*, 2013, **19**, 327–336.
12 S. Hashimoto, *Soil Biol. Biochem.*, 2002, **34**, 273–275.
13 E. R. Crosson, *Appl. Phys. B: Lasers Opt.*, 2008, **92**, 403–408.
14 A. J. Rixon and B. J. Bridge, *Nature*, 1968, **218**, 261–262.
15 R. A. Halvorson and P. J. Vikesland, *Environ. Sci. Technol.*, 2010, **44**, 7749–7755.
16 T. Frosch, D. Yan and J. Popp, *Anal. Chem.*, 2013, **85**, 6264–6271.
17 T. Frosch, S. Koncarevic, L. Zedler, M. Schmitt, K. Schenzel, K. Becker and J. Popp, *J. Phys. Chem. B*, 2007, **111**, 11047–11056.
18 T. Frosch, T. Meyer, M. Schmitt and J. Popp, *Anal. Chem.*, 2007, **79**, 6159–6166.
19 P. J. Hendra and C. J. Vear, *Analyst*, 1970, **95**, 321–342.
20 T. Frosch and J. Popp, *J. Mol. Struct.*, 2009, **924–926**, 301–308.
21 T. Frosch, S. Koncarevic, K. Becker and J. Popp, *Analyst*, 2009, **134**, 1126–1132.
22 R. Keiner, T. Frosch, S. Hanf, A. Rusznyak, D. M. Akob, K. Kusel and J. Popp, *Anal. Chem.*, 2013, **85**, 8708–8714.
23 S. Hanf, T. Bögözi, R. Keiner, T. Frosch and J. Popp, *Anal. Chem.*, 2015, **87**(2), 982–988.
24 T. Bögözi, J. Popp and T. Frosch, *Bioanalysis*, 2015, **7**(3), 281–284.
25 R. Keiner, M.-C. Gruselle, B. Michalzik, J. Popp and T. Frosch, *Anal. Bioanal. Chem.*, 2015, **407**, 1813–1817.
26 S. Hanf, R. Keiner, D. Yan, J. Popp and T. Frosch, *Anal. Chem.*, 2014, **86**, 5278–5285.
27 IUSS Working Group WRB, in World Soil Resources Reports No. 103, FAO, Rome, 2006.
28 R. Keiner, T. Frosch, T. Massad, S. Trumbore and J. Popp, *Analyst*, 2014, **139**(16), 3879–3884.
29 T. Frosch, R. Keiner, B. Michalzik, B. Fischer and J. Popp, *Anal. Chem.*, 2013, **85**, 1295–1299.
30 D. A. King and R. J. Pittaro, *Opt. Lett.*, 1998, **23**, 774–776.
31 T. Naganawa and K. Kyuma, *Soil Sci. Plant Nutr.*, 1991, **37**, 381–386.
32 F. Mavituna and B. Atkinson, *Biochemical engineering and biotechnology handbook*, Nature Press, New York, NY, 1983.
33 P. Du, M. Sagehashi, A. Terada, S. Zhou, F. S. Li and M. Hosomi, *Soil Sci. Soc. Am. J.*, 2011, **75**, 2147–2157.
34 T. H. Wiedemeier, J. T. Wilson, D. H. Kampbell, R. N. Miller and J. E. Hansen, *Technical Protocol for Implementing Intrinsic Remediation with Long-Term Monitoring for Natural Attenuation of Fuel Contamination Dissolved in Groundwater. Volume II*, DTIC Document, 1995.
35 H. F. Birch, *Nature*, 1958, **182**, 1172.
36 H. F. Birch, *Plant Soil*, 1959, **IX**, 262–286.
37 O. Dilly, S. Nii-Annang, G. Franke, T. Fischer, F. Buegger and A. Zyakun, *Soil Biol. Biochem.*, 2011, **43**, 1808–1811.

38 E. A. Steinhaus and J. M. Birkeland, *J. Bacteriol.*, 1939, **38**, 249–261.
39 F. Scheffer and P. Schachtschabel, *Lehrbuch der Bodenkunde*, Spektrum Akademischer Verlag, Heidelberg, 2010.
40 R. W. O'Dowd and D. W. Hopkins, *Soil Biol. Biochem.*, 1998, **30**, 2009–2016.
41 K. Haider, G. Jagnow, R. Kohnen and S. U. Lim, *Arch. Microbiol.*, 1974, **96**, 183–200.
42 W. X. Zhang and E. J. Bouwer, *Biodegradation*, 1997, **8**, 167–175.
43 E. Lamy, T. C. Tran, S. Mottelet, A. Pauss and O. Schoefs, *Int. Biodeterior. Biodegrad.*, 2013, **83**, 85–91.
44 P. D. Golding and W. D. Machin, *J. Chem. Soc., Faraday Trans. 1*, 1987, **83**, 2719–2726.
45 D. R. Shonnard and R. L. Bell, *Environ. Sci. Technol.*, 1993, **27**, 2909–2913.
46 E. A. Voudrias and C. Y. Li, *J. Hazard. Mater.*, 1993, **34**, 295–311.
47 R. Arands, T. Lam, I. Massry, D. H. Berler, F. J. Muzzio and D. S. Kosson, *Water Resour. Res.*, 1997, **33**, 599–609.